cmgh
CELLULAR AND MOLECULAR GASTROENTEROLOGY AND HEPATOLOGY

ORIGINAL RESEARCH

Intrahepatic Exhausted Antiviral Immunity in an Immunocompetent Mouse Model of Chronic Hepatitis B

Satoshi Shigeno,[1,*] Takahiro Kodama,[1,*] Kazuhiro Murai,[1] Daisuke Motooka,[2] Akihisa Fukushima,[3] Akira Nishio,[1] Hayato Hikita,[1] Tomohide Tatsumi,[1] Toru Okamoto,[4] Tatsuya Kanto,[5] and Tetsuo Takehara[1]

[1]Department of Gastroenterology and Hepatology, Osaka University Graduate School of Medicine, Suita, Japan; [2]Genome Information Research Center, Research Institute for Microbial Diseases, Osaka University, Suita, Japan; [3]Vaccines, Sumitomo Pharma Co., Ltd., Osaka, Japan; [4]Institute for Advanced Co-Creation Studies, Research Institute for Microbial Diseases, Osaka University, Suita, Japan; and [5]The Research Center for Hepatitis and Immunology, National Center for Global Health and Medicine, Ichikawa, Chiba, Japan

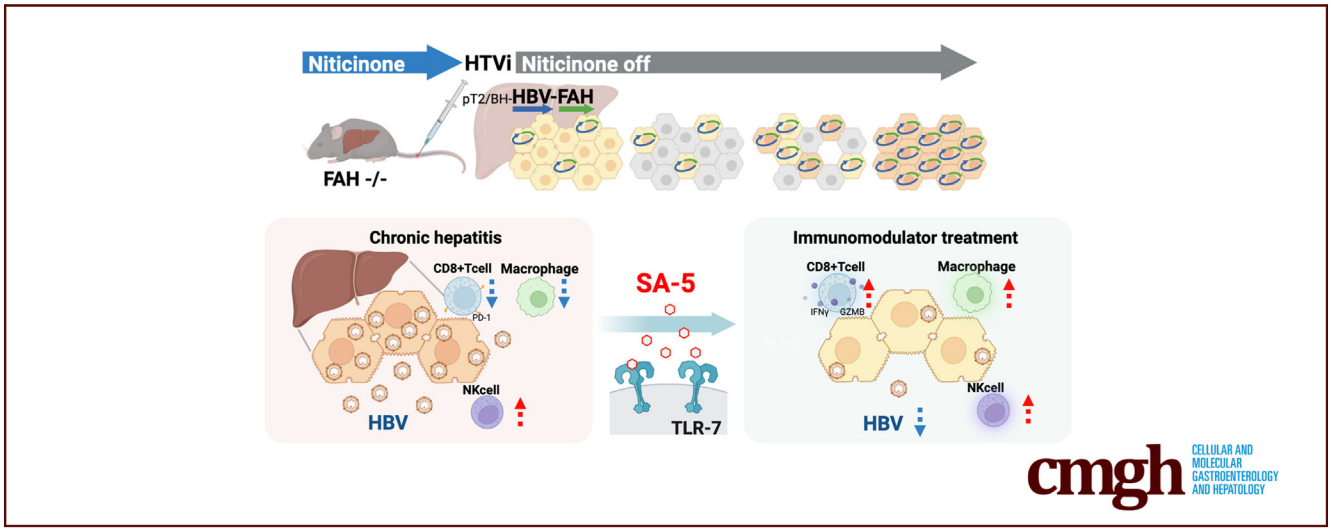

SUMMARY

Our novel immunocompetent mouse model recapitulated the intrahepatic exhausted antiviral immunity in patients with chronic hepatitis B, which might be able to be reinvigorated by a hepatotropic TLR7 agonist.

BACKGROUND & AIMS: Targeting exhausted immune systems would be a promising therapeutic strategy to achieve a functional cure for HBV infection in patients with chronic hepatitis B (CHB). However, animal models recapitulating the immunokinetics of CHB are very limited. We aimed to develop an immunocompetent mouse model of CHB for intrahepatic immune profiling.

METHODS: CHB mice were created by intrahepatic delivery of the Sleeping Beauty transposon vector tandemly expressing the hepatitis B virus (HBV) genome and fumarylacetoacetate hydrolase (FAH) cDNA into C57BL/6J congenic FAH knockout mice via hydrodynamic tail vein injection. We profiled the viral and intrahepatic immune kinetics in CHB mice with or without treatment with recombinant IFNα or the hepatotropic Toll-like receptor 7 agonist SA-5 using single-cell RNA-seq.

RESULTS: CHB mice exhibited sustained HBV viremia and persistent hepatitis. They showed intrahepatic expansion of exhausted CD8+ T (Tex) cells, the frequency of which was positively associated with viral load. Recruited macrophages increased in number but impaired inflammatory responses in the liver. The cytotoxicity of mature natural killer (NK) cells also increased in CHB mice. IFNα and SA-5 treatment both resulted in viral suppression with mild hepatic flares in CHB mice. Although both treatments activated NK cells, SA-5 had the capacity to revitalize the impaired function of Tex cells and liver-recruited macrophages.

CONCLUSION: Our novel CHB mouse model recapitulated the intrahepatic exhausted antiviral immunity in patients with CHB, which might be able to be reinvigorated by a hepatotropic TLR7 agonist. *(Cell Mol Gastroenterol Hepatol 2025;19:101412; https://doi.org/10.1016/j.jcmgh.2024.101412)*

Keywords: Chronic Hepatitis B; HBV; Immunocompetent; Mouse Model.

This article has an accompanying editorial.

Hepatitis B virus (HBV) is a highly prevalent infectious disease globally, with approximately 296 million people chronically infected worldwide. Chronic infection may last for a lifetime and cause liver cirrhosis and/or hepatocellular carcinoma, which makes HBV the most common pathogen of death among patients with viral hepatitis, with a reported incidence of 820,000 per year.[1]

The natural history of chronic hepatitis B (CHB) follows several clinical phases depending on the states of host immune responses and viral replication. The immune-tolerant phase is defined by high viral replication but minimal inflammation. The immune-active phase is characterized by elevated serum alanine aminotransferase (ALT) levels with persistent liver necroinflammation. As HBV is not directly cytopathic, host responses are thought to mediate liver pathogenesis and contribute to the development of cirrhosis and liver cancer in the immune active phase.[2–4] In patients with CHB, current antiviral therapies such as nucleotide/nucleoside analogs (NAs) can inhibit the replication of HBV and alleviate liver injury; however, in most cases, they hardly eliminate the virus itself from hepatocytes.[5,6] Some hepatic immune cells have been reported to contribute to the persistence of viral infection. CD8+ T cells are believed to be necessary for the elimination of HBV but often have an impaired capacity for proliferation and cytotoxic activity.[7,8] The dual nature of macrophages is reported to contribute to persistent HBV infection.[9,10] Although pro-inflammatory macrophage cytokine secretions can inhibit viral infection, the virus's modulation of macrophage phenotypes promotes the establishment and persistence of the infection. Although these insufficient immune responses have been highlighted as prospective targets for virus elimination,[5,7] the comprehensive immune dynamics involved in patients with CHB have not been fully elucidated.

To clarify the immunopathology of patients with CHB and investigate immunomodulatory agents aimed at HBV elimination, it is critical to develop animal models that recapitulate chronic HBV infection and the host immune response in patients with CHB. HBV is a highly species-specific virus, and the only animals known to be susceptible to human HBV are chimpanzees and tree shrews, which are not readily accessible for use in experiments. Transgenic (Tg) mouse models expressing HBV have significantly contributed to understanding viral mechanisms; however, these models are naturally immunotolerant to HBV and thus cannot be used for the study of immunopathology. In the transfected mouse model, hydrodynamic injection is used to transfer the HBV-expressing vectors into the liver, resulting in transient high levels of HBV replication. However, they have been utilized as a model to mimic the pathogenesis of acute hepatitis rather than chronic hepatitis. Several models, such as the adeno-associated virus (AAV)-mediated transfected model, have persistent viremia; however, they originally lack active immune responses and recapitulate the immune-tolerant phase in humans.[11–14] Adaptive transfer of immune cells from HBV-specific T cell receptor (TCR)-Tg mice into major histocompatibility complex (MHC) class I-matched HBV-Tg mice is a sophisticated strategy that can be used to study how naïve T cells respond to HBV in vivo, but the model does not fully recapitulate physiological T cell biology in terms of external transfer of T cells into the body.[15] Recently developed dual chimeric mouse models harboring human hepatocytes and the hematopoietic system are expected to facilitate the understanding of viral immune pathophysiology but still have considerable difficulties in generation and cost.[16–18] For the discovery of effective immunomodulatory therapeutics, appropriate immunocompetent animal models of CHB are desperately needed.

To this end, we aimed to establish a novel immunocompetent mouse model of CHB with a simple combination of a fumarylacetoacetate hydrolase (FAH)-knockout (KO) mouse, hydrodynamic tail vein injection (HTVi), and a Sleeping Beauty (SB) transposon system. FAH-KO mouse is a model animal for tyrosinemia that suffers from fatal hepatic damage not supplied with nitisinone (NTBC) in the drinking water, and this feature makes it possible to control the death of FAH-deficient hepatocytes. Through the genomic integration of a single SB vector constitutively expressing FAH and HBV, the proliferating potential of FAH-proficient hepatocytes in FAH-KO mice enabled the persistent expansion of HBV-expressing hepatocytes throughout the liver. With this model, we profiled immunokinetics during chronic HBV infection and investigated the intrahepatic immune response towards immunomodulatory agents, including clinically applicable interferon alpha (IFNα) and novel hepatotropic Toll-like receptor (TLR) 7 agonists in development.

***Authors share co-first authorship.**

Abbreviations used in this paper: **AAV, adeno-associated virus; ALT, alanine aminotransferase; ANOVA, analysis of variance; cccDNA, covalently closed circular DNA; cDC, conventional dendritic cell; cDNA, complementary DNA; CHB, chronic hepatitis B; CMV, cytomegalovirus; FACS, fluorescence-activated cell sorting; FAH, fumarylacetoacetate hydrolase; GSEA, gene set enrichment analysis; GZM, granzyme; GVHD, graft-vs-host disease; H&E, hematoxylin and eosin; HBcAg, hepatitis B core antigen; HBeAg, hepatitis B e antigen; HBsAg, hepatitis B surface antigen; HBV, hepatitis B virus; HTVi, hydrodynamic tail vein injection; IFN, interferon; KC, Kupffer cell; KO, knockout; LLOQ, lower limit of quantification; mAb, monoclonal antibody; MHC, major histocompatibility complex; MNC, mononuclear cell; NA, nucleic acid analogue; NK, natural killer; NTBC, nitisinone; NTCP, sodium taurocholate cotransporting polypeptide; RBC, red blood cell; PBS, phosphate buffered saline; pDC, plasmacytoid dendritic cell; PD-1, programmed cell death 1; PMA, phorbol myristate acetate; pgRNA, pregenomic RNA; RT–PCR, reverse transcription polymerase chain reaction; SB, Sleeping Beauty; scRNA-seq, single-cell RNA sequencing; SD, standard deviation; 7AAD, 7-aminoactinomycin D; TCR, T cell receptor; Teff, effector memory T; Tex, exhausted T; Tfh, T follicular helper; Tg, transgenic; TLR7, Toll-like receptor 7; Tn, naïve T; TNF, tumor necrosis factor; Treg, regulatory T; TUNEL, terminal deoxynucleotidyl transferase dUTP nick end labeling; WTA, whole-transcriptome analysis; UMAP, uniform manifold approximation and projection.**

Most current article

2352-345X
https://doi.org/10.1016/j.jcmgh.2024.101412

Results

Intrahepatic Delivery of Transposon-based Tandem HBV- and FAH-expressing Vectors in FAH-KO Mice Recapitulates the Immune Active Phase of CHB

To generate an immunocompetent CHB mouse model, we aimed to deliver a plasmid that expresses FAH and HBV in tandem into the liver genome in C57BL/6J congenic FAH-KO mice. To this end, the cytomegalovirus (CMV) promoter-driven full-length FAH sequence was first inserted into the SB vector generated from pT2/BH (pT2/BH-FAH). The 1.24-mer overall length HBV genome was subsequently inserted into pT2/BH-FAH in tandem (pT2/BH-HBV-FAH). As a control plasmid, only the HBV genome or FHA cDNA was inserted into pT2/BH (pT2/BH-HBV) (Figure 1*A*). We then introduced each vector into the liver via HTVi (Figure 1*B*). Upon HTVi, NTBC withdrawal led to approximately 30% weight loss in all the FAH-KO mice (Figure 1*C*). The FAH-KO mice with pT2/BH-HBV could not recover their lost weight, and all died (Figure 1*C*). Meanwhile, the FAH-KO mice with pT2/BH-HBV-FAH regained their weight to the same level as that of the FAH-KO mice with NTBC drinking (Figure 1*C*), suggesting that intrahepatic delivery of the FAH-expressing vector rescued the lethal phenotype of FAH-KO mice induced by NTBC withdrawal. Upon HTVi of the HBV-expressing vector (pT2/BH-HBV-FAH or pT2/BH-HBV), all the mice showed HBV viremia exhibited by the increase in serum hepatitis B surface antigen (HBsAg), and HBV-DNA levels (Figure 1*D, E*). However, by 4 weeks after HTVi, the serum viral expression decreased to below the lower limit of quantification (LLOQ) in all the mice except those transfected with pT2/BH-HBV-FAH and withdrawn from NTBC (named CHB mice hereafter), exhibiting persistent elevation of serum HBsAg and HBV-DNA levels during the longest observation period of up to 25 weeks post-HTVi (Figure 1*D, E*). Hepatitis B e antigen (HBeAg) was also detected in the serum of CHB mice (Figure 1*F*). HBsAg expression was only observed in the liver but not in other major organs, suggesting the specific transposition of SB vector in the liver upon HTVi (Figure 1*G*). Approximately 80% of hepatocytes were positive for FAH, and the median 2.5 copies of transposon were integrated in the hepatocytes without silencing of CMV promoter-driven FAH expression over time in the CHB mice (Figure 1*H–K*).

We next evaluated phenotypes in the livers of the CHB mice and their control FAH-KO mice with the pT2/BH-FAH vector. pgRNA was detectable in the livers of CHB mice (Figure 1*L*). Immunohistochemical analysis showed that HBsAg was expressed in the FAH-expressing hepatocytes throughout the liver (Figure 1*M*). Approximately 2 to 4 weeks after HTVi, serum ALT levels were elevated to approximately 700 U/L in both the CHB mice and the control mice (Figure 1*N*). After the ALT levels of the control mice became below the normal limit (<40 U/L), the ALT elevation of CHB mice continued at approximately 150 U/L over the observation period (Figure 1*N*). The CHB mice showed intrahepatic infiltration of inflammatory cells, elevation of the histopathological inflammatory score, increases in the numbers of terminal deoxynucleotidyl transferase dUTP nick end labeling (TUNEL)-positive hepatocytes, and elevations in serum caspase 3/7 activity (Figure 1*O–S*), suggesting chronic liver necroinflammation caused by immune cells recognizing HBV-infected hepatocytes in CHB mice.

Single-cell Landscape of Intrahepatic Immune Cells in CHB Mice

To understand the immunopathology of the liver in our CHB mice, hepatic immune cells were analyzed by single-cell RNA sequencing (scRNA-seq) at the chronic inflammation phase (8 weeks after HTVi). A total of 13,743 cells from 6 CHB mice and 10,680 cells from 4 control mice were classified into 33 clusters, which could be defined as 11 major cell types, including CD8+ T cells, CD4+ T cells, natural killer (NK) cells, macrophages, conventional dendritic cells (cDCs), plasmacytoid dendritic cells (pDCs), B cells, monocytes, neutrophils, mast cells, and hepatocytes (Figure 2*A*) based on the expression of characteristic marker genes (Figure 2*B*). Both groups of HBV and control mice had cells in each major cluster, but there was no difference in their frequency (Figure 2*C*).

The Exhaustion of Intrahepatic CD8+ T cells May Contribute to Persistent HBV Viremia in CHB Mice

We then focused on CD8+ T cells and further divided them into 4 subclusters, including naïve T (Tn) cells, effector memory T (Tem) cells, effector T (Teff) cells, and exhausted T (Tex) cells (Figure 2*D*), based on the expression of characteristic marker genes such as *Lef1*, *Sell*, and *Ccr7* in Tn cells; Ly6c2, and *Fcgr3*, in Tem cells; *Cxcr3*, *Cd160,* and *Itga1* in Teff cells; and *Pdcd1* and *Tox* in Tex cells (Figure 2*E*). We performed pseudotime analysis with the Monocle algorithm to elucidate trajectories across cell states,[19] revealing the differentiation process of CD8+ T cells (purple to yellow) (Figure 2*F*), progressing from Tn to Tem or Teff cells, and finally to Tex cells, which were more prominent in the livers of CHB mice than in the livers of FAH mice (Figure 2*F–H*). Increase in the exhaustion of CD8 T cells was unique in the liver and not observed in the circulation of the CHB mice (Figure 2*I*). Alterations in individual gene expression over the pseudo-time course showed a gradual elevation of *Tox* in the exhausted state (Figure 2*J*). *IL7r*, which is crucial for the development of various immune cells, showed a decreasing trend in the late phase (Figure 2*J*). Importantly, the Tex cells in the CHB mice showed significantly higher mRNA levels of *Pdcd1* and *Tox* than the Tex cells in the control mice (Figure 2*K*). These data suggested that the CHB mice had more intrahepatic Tex cells and greater exhaustion of these cells than control mice. Flow cytometry of intrahepatic CD8+ T cells in the CHB mice showed a strong positive correlation between the frequency of programmed cell death 1 (PD-1)+CD8+ T cells and viral expression of serum HBsAg and HBV-DNA (Figure 2*L*). These data suggested that the exhaustion of CD8+ T cells may be closely related to persistent HBV viremia in CHB mice.

The frequency of PD-1+CD8+ T cells and Tim-3+CD8+ T cells were found to increase with age (Figure 2*M*), suggesting that immunological exhaustion of CD8+ T cells became deeper with age. We also evaluated the HBV-specific T cells by the tetramers of H-2K^{b}-restricted HBV-derived epitopes. We were able to detect the HBV-specific T cells for both HBsAg and hepatitis B core antigen (HBcAg), and their frequencies were higher in the liver compared with

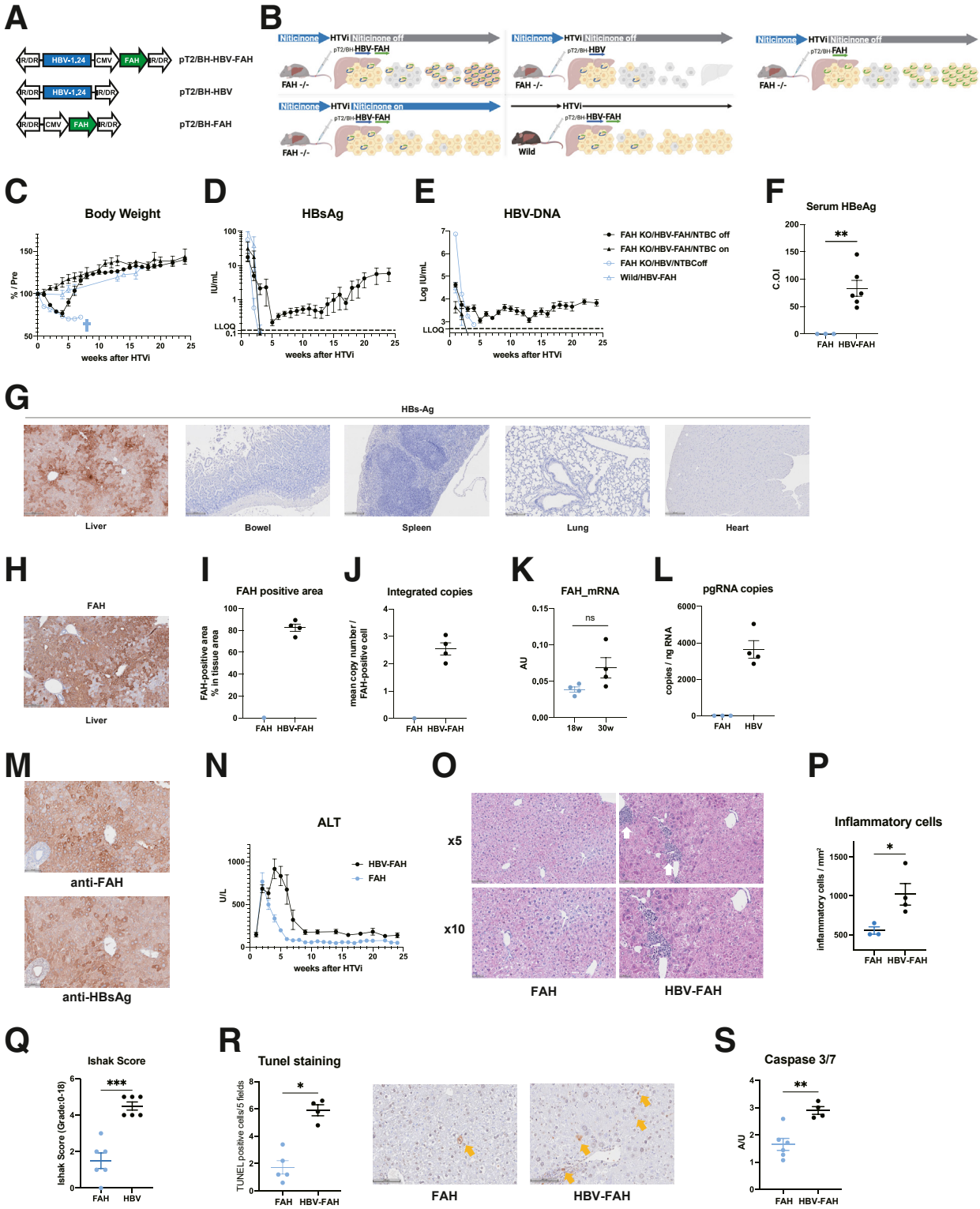

those in the spleen and peripheral blood (Figure 2*N*). In addition, the frequency of PD-1-positive cells in the HBV-specific CD8+ T cells was significantly higher than that in the non-specific CD8+ T cells, whereas the frequency of IFNγ+ (tumor necrosis factor) TNFα+ cells in the HBV-specific CD8+ T cells was also significantly lower than that in the non-specific CD8+ T cells in CHB mice (Figure 2*O*). These results further supported the HBV-specific immunological exhaustion of CD8+ T cells in the liver of our CHB model.

Dysfunction of the Recruited Macrophages in the Livers of CHB Mice

Next, we focused on the macrophage clusters that contained 2 subclusters as resident Kupffer cells (KCs) and recruited macrophages (Figure 3*A*). Resident KCs were characterized by the coexpression of *Clec4f*, and *Clec2d*, and recruited macrophages were characterized by coexpression of *Ccr2, Itgam*, *Ly6c1*, and *Ly6c2* (Figure 3*B*). The frequency of recruited macrophages was significantly higher in the livers of CHB mice than in those of control mice (Figure 3*C*). Compared with those in the control mice, the recruited macrophages in the CHB mice showed significant down-regulation of genes related to antigen-presentation such as *Cd74* and *H2-Aa*; significant upregulation of anti-inflammatory modulators such as *Klf2* and *Klf4* (Figure 3*D*); and significantly reduced inflammatory response scores (Figure 3*E*). Gene set enrichment analysis (GSEA) showed the negative enrichment scores for multiple pathways related to the immune and defense responses in the CHB mice compared with those in the control mice, suggesting the suppression of these pathways (Figure 3*F, G*). These findings suggested dysfunction of the recruited macrophages in CHB mice.

We further investigated the cell–cell interactions between T cells (including CD8+ T cells and CD4+ T cells) and macrophage clusters. CellChat analysis identified that the recruited macrophages in the CHB mice had a higher differential number of interactions than those in the control mice, especially with Tex and Tem clusters (Figure 3*H*). Focusing on the interaction strength from 2 macrophage clusters to T cell clusters, strong cell–cell interactions from recruited macrophages and resident KCs to the Tex cluster were observed in the CHB mice (Figure 3*I*). These data suggested that macrophages might be involved in the exhaustion of CD8+ T cells in CHB mice.

Activation of Mature NK Cells in the Livers of CHB Mice

We then focused on NK cells that were divided into 2 subclusters according to maturation status (Figure 4*A*). Mature NK cells were characterized by the coexpression of *Itgam* and *Klrg1,* and immature NK cell clusters were characterized by the coexpression of *Cd27* and *Foxo1* (Figure 4*B*). Pseudotime analysis showed the gradual maturation process of NK cells (purple to yellow) from the immature state to the mature state (Figure 4*C*). Compared with the mature NK cells in the control mice, the mature NK cells in the livers of CHB mice expressed significantly higher levels of *Gzma* and *Gzmb*, and had significantly higher cytotoxic scores (Figure 4*D, E*), suggesting the activation of NK cells in the CHB mice. Consistently, flow cytometry revealed that the frequency of intrahepatic IFNγ+ NK cells was significantly higher in the CHB mice than in the control mice (Figure 4*F*).

Immunomodulatory Agents Induce the Intrahepatic Immune Response and Viral Suppression in CHB Mice

Based on the immunokinetics of the CHB mice that recapitulate the immune active phase of CHB in humans, we decided to use this model to examine the intrahepatic immune response to IFNα, available in clinical practice, and SA-5, a novel TLR7 agonist under clinical development. SA-5 is an orally active small molecule TLR7 agonist that is an analogue to Guretolimod (DSP-0509), a pyrimidine derivative.[20] Daily subcutaneous administration of recombinant IFNα (10,000 U per mouse) in the CHB mice significantly suppressed the serum HBV-DNA levels and hepatic pgRNA levels (Figure 5*A, B*), whereas it induced mild liver damage exhibited by the 2- to 3-fold increase in the serum ALT levels (Figure 5*C*). The FAH levels were not altered by IFNα treatment (Figure 5*D*). The anti-viral effect of IFNα was similar to the one obtained by the nucleotide analogue in the CHB mice (Figure 5*E*). IFNα treatment significantly increased the

Figure 1. (***See previous page***). **Intrahepatic delivery of a transposon-based tandem HBV and FAH expressing vector in the FAH-KO mice recapitulates the immune active phase of CHB.** (*A*) Design of each HBV vector. Either the 1.24-mer overall length of the HBV genome or CMV promoter-driven FAH cDNA or both were cloned into a single SB transposon vector. (*B*) Experimental scheme including FAH-KO mice with HBV-FAH and without NTBC (*upper left*), FAH-KO mice with HBV-FAH and with NTBC (*lower left*), FAH-KO mice with HBV and without NTBC (*upper middle*), wild-type mice with HBV-FAH (*lower middle*), and FAH-KO mice with FAH and without NTBC (*upper right*) (n = 3–5 mice per group). (*C*) Body weight of mice after HTVi. (*D–F*) Serum HBsAg (*D*), HBV DNA (*E*), and HBeAg (*F*) levels after HTVi. (*G*) Immunohistochemical staining for HBs antigen in the liver, bowel, spleen, lung, and heart tissues of the FAH-KO mice with HBV-FAH and without NTBC. (*H*) Immunohistochemical staining for FAH in the liver of the FAH-KO mice with HBV-FAH and without NTBC. (*I*) The positive area of FAH in the liver of the FAH-KO mice with HBV-FAH and without NTBC. (*J*) The median copy number of transposon integrated into the hepatocytes. (*K*) FAH mRNA levels in the liver of the FAH-KO mice with HBV-FAH and without NTBC at 18 or 30 weeks of age. (*L*) pgRNA copies in hepatocytes. (*M*) Immunohistochemical staining for FAH and HBs antigen in liver tissues. (*N*) Serum ALT levels after HTVi. (*O*) H&E staining of liver sections. The *white arrow* indicates inflammatory cells. (*P*) Number of inflammatory cells detected by H&E staining. (*Q*) The ISHAK histopathological inflammatory score assessed by H&E staining. (*R*) TUNEL-positive cells in TUNEL staining of liver sections. (*S*) Serum caspase-3/7 activity. AU, Arbitrary unit. *$P < .05$; **$P < .01$; ***$P < .001$.

intrahepatic mRNA levels of *Isg15*, *Oas2*, and *Gzmb* in the CHB mice (Figure 5*F*). Similarly, oral administration of SA-5 in the CHB mice significantly suppressed the serum HBV-DNA levels and hepatic pgRNA levels (Figure 5*G, H*) with transient elevation of the serum ALT levels up to 4-fold (Figure 5*I*). SA-5 treatment also significantly increased the intrahepatic mRNA levels of *Isg15*, *Oas2*, and *Gzmb* in the CHB mice (Figure 5*J*). To evaluate the durability of the antiviral response, we treated HBV-FAH animals for 3 weeks by IFN or SA-5. We found that the antiviral response was maintained at a similar strength during the longer treatment duration (Figure 5*K*). These data suggested that immunomodulatory agents induced an intrahepatic immune response and viral suppression in CHB mice.

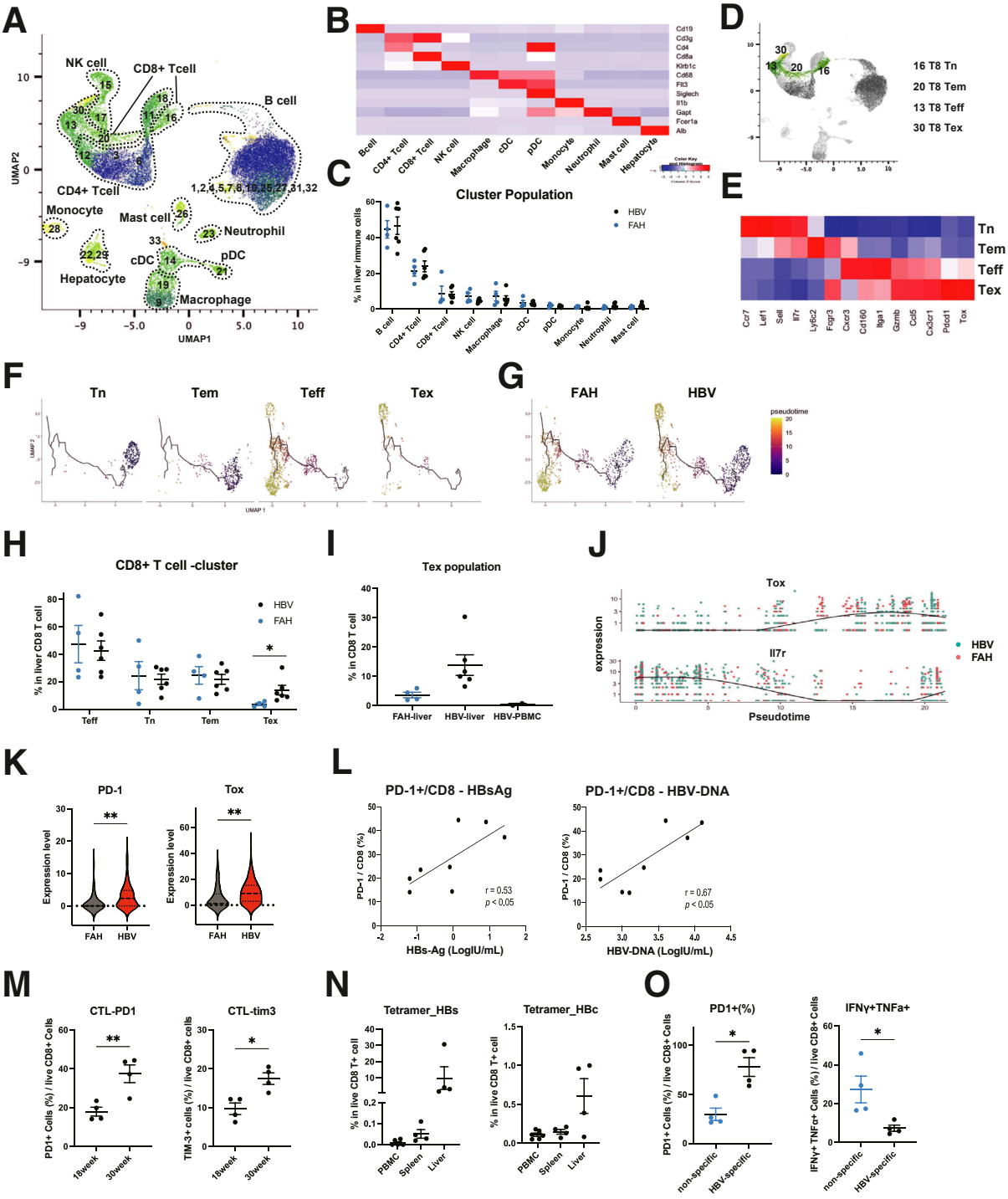

Immunomodulatory Effects of IFNα and SA-5 in CHB Mice

Finally, we investigated the global landscape of intrahepatic immune cells in CHB mice treated with immunomodulatory agents. scRNA-seq data from 3 IFNα-treated mice and 3 SA-5-treated mice were integrated with those from nontreated CHB mice and control mice. A total of 36,670 cells, including 6607 cells from IFNα-treated mice and 5671 cells from SA-5-treated mice, were classified into 11 major cell types, as in the original dataset. Both IFNα and SA-5 induced Isg15 expression in various immune cells including macrophage, cDC, and monocytes (Figure 6*A*). Regarding CD8+ T cells, although IFNα treatment activated Tem, Teff, and Tex cells, but not Tn cells, as exhibited by the IFNγ signaling score (Figure 6*B*), SA-5 treatment activated all types of CD8+ T cells, and the IFNγ signaling scores of Tn, Teff, and Tex cells were significantly higher in SA-5-treated mice than in all other mice (Figure 6*B*). Although both IFNα and SA-5 activated macrophages and NK cells compared with the control mice, inflammatory response score in recruited macrophages and cytotoxic score in NK cells were significantly higher in SA-5-treated mice than in all other mice (Figure 6*C, D*). Consistent with these findings, flow cytometry showed that both IFNα and SA-5 treatment increased the population of IFNγ+Gzmb+ NK cells in the livers of CHB mice, whereas only SA-5 treatment increased the population of IFNγ+Gzmb+ CD8+ T cells (Figure 6*E, F*). Taken together, the findings indicated that SA-5 treatment activated a wide variety of intrahepatic immune cells with viral suppression in CHB mice, suggesting its potential as a promising immunomodulatory therapeutic for CHB.

Discussion

In this study, we established a novel immunocompetent mouse model of CHB with the characteristics of the immune-active phase of human CHB. The employment of scRNA-seq in this model revealed the intrahepatic immune landscape contributing to the persistence of HBV infection at single-cell resolution. Our model also made it possible to profile the intrahepatic immune response to immunomodulators, shedding light on the potential of the hepatotropic TLR-7 agonist SA-5 as a drug that activates anti-HBV immunity, which is important for viral elimination.

Our CHB mouse model has a unique mechanism that enables viral persistence under immunocompetent circumstances. This model, similar to most HBV mouse models except humanized models, does not mimic the entry of the HBV into hepatocytes, which is mediated by sodium taurocholate cotransporting polypeptide (NTCP), as in the human liver.[21] Instead, through the genomic integration of a single SB vector constitutively expressing FAH and HBV, the proliferating potential of only FAH-proficient hepatocytes in FAH-KO mice[22] enabled the persistent expansion of HBV-expressing hepatocytes throughout the liver. The presence of covalently closed circular DNA (cccDNA) is considered one of the reasons for the difficulty of eliminating HBV.[23] Our model may not be appropriate for studying cccDNA biology but recapitulates integrated HBV DNA, which has been recently recognized as an important source of viral proteins and another hindrance to a functional cure.[23] Recently developed dual humanized mouse models harboring human hepatocytes and hematopoietic systems are expected to mimic viral immunopathology in humans.[17] Some of these dual humanized mouse models have adopted the FAH-KO system, like our model, to enable suitable engraftment of human transplants.[17] The caveat of these models is the exogenous transplantation system and species heterogeneity, that is, the simultaneous presence of cells from different species (humans and mice) in the liver. Because humanized mouse models were originally utilized for research on graft-vs-host disease (GVHD), the dual chimeric humanized mouse model of HBV may consist of the exquisite balance between the potential risk of GVHD and HBV-specific immune reactions. In this sense, despite species differences, our model has the advantage of enabling assessment of endogenous chronic immune responses to virus-expressing hepatocytes.

Our CHB mice recapitulated several important immunological features observed in patients with CHB. CD8+ T cells are thought to be primary effectors for viral clearance and hepatitis during HBV infection,[24] but T cell responses are often impaired in patients with CHB.[25] Recent studies on human samples at single-cell resolution have suggested that Tex cells are preferentially expanded in the immune active phase,[26] which is in agreement with our findings in CHB mice. The positive correlation between PD-1 expression in CD8+ T cells and the viral load in our mice further

Figure 2. (***See previous page***). **Single-cell atlas of intrahepatic immune cells and the exhaustion of CD8+ T cells in CHB mice.** (*A–J*) Hepatic immune cells from CHB mice and control mice at 8 weeks post-HTVi were analyzed by scRNA-seq (n = 6 for CHB mice and n = 4 for control mice). (*A*) A total of 24,423 cells were classified into 33 clusters described by UMAP that could be unified into 11 major clusters. (*B*) Heatmap showing the expression levels of representative genes for each cell type. (*C*) The population of each major cluster. (*D–E*) Four CD8+ T cell subsets in UMAP (*D*) were defined by indicated marker gene expression patterns shown in the heatmap (*E*). (*F–G*) Pseudotime trajectory analysis of 4 CD8+ T cell subsets. (*H*) The population of each cluster of 4 CD8+ T cell subsets. (*I*) The population of exhausted CD8+ T cell subsets in the liver of CHB mice and control mice and PBMC of CHB mice. (*J*) Expression levels of *Il7r* and *Tox* at each pseudotime point in 4 CD8+ T cell subsets. (*K*) Violin plots showing the expression levels of *PD-1* and *Tox* in Tex. (*L*) The correlation between the frequency of intrahepatic PD-1+CD8+ T cells determined by flow cytometry and the serum HBsAg and HBV-DNA levels. (*M*) The frequency of intrahepatic PD-1+CD8+ T cells and Tim-3+CD8+ T cells among all CD8+ T cells at 18 or 30 weeks of age in the liver of CHB mice determined by flow cytometry. (*N*) The frequency of HBV-specific T cells for either HBsAg and HBcAg in the liver, spleen, and PBMC of the CHB mice determined by flow cytometry. (*O*) The frequency of PD-1+ cells and IFNγ+TNFα+ cells in the HBV-specific and non-specific CD8+ T cells in the liver of CHB mice determined by flow cytometry. $^{*}P < .05$; $^{**}P < .01$. Nn, Naïve T cell; Tem, effector memory T cell; Teff, effector T cell; Tex, exhausted T cell.

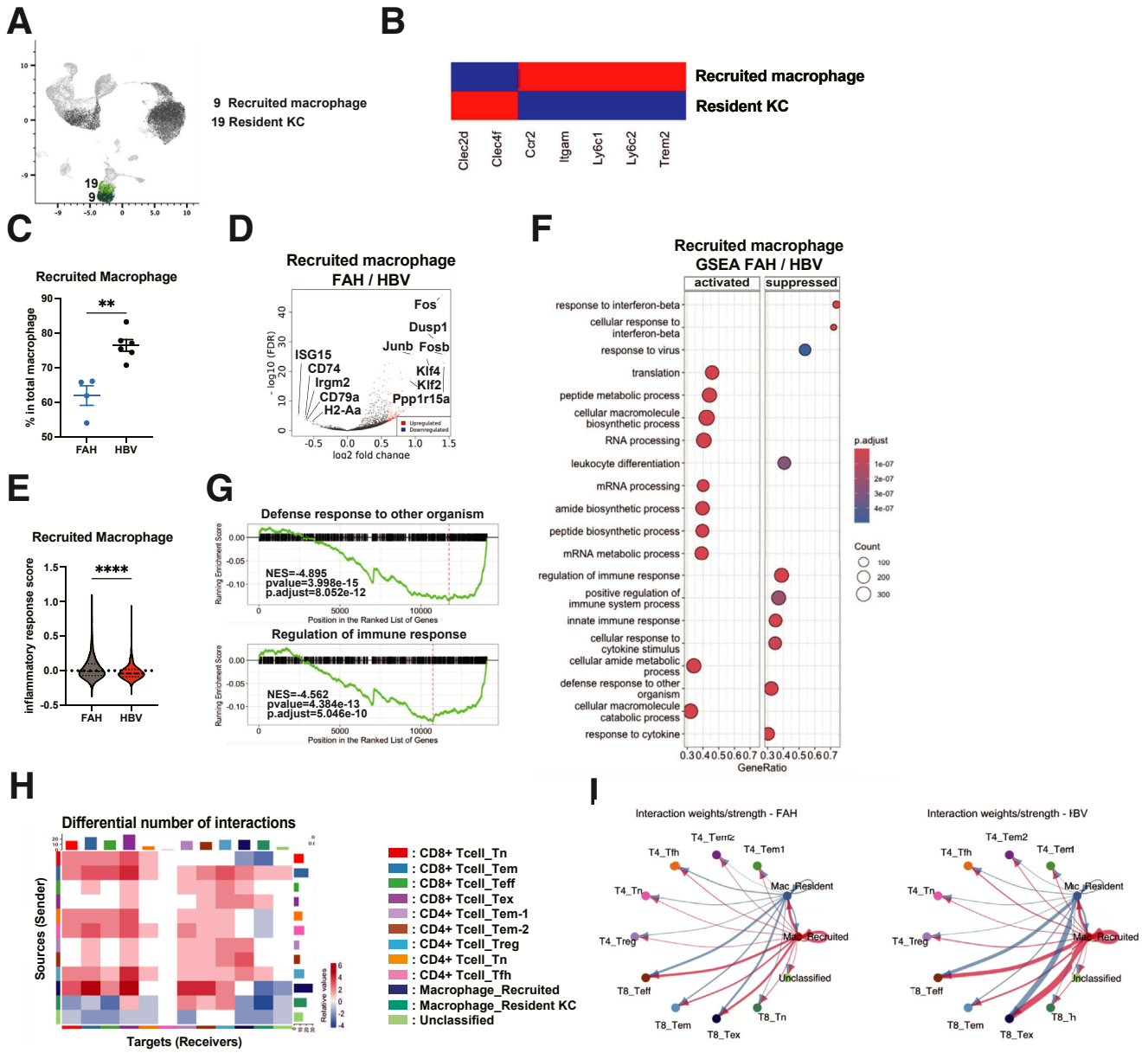

Figure 3. Dysfunction of the recruited macrophages in the livers of CHB mice. (*A–I*) Hepatic immune cells from CHB mice and control mice at 8 weeks post-HTVi were analyzed by scRNA-seq sequencing (n = 6 for CHB mice and n = 4 for control mice). (*A–B*) Two macrophage subsets in UMAP (*A*) were defined by the indicated marker gene expression shown in the heatmap (*B*). (*C*) The population ratio of recruited macrophages to resident KCs. (*D*) Volcano plot of differential gene expression of recruited macrophages (FAH vs HBV). (*E*) Violin plot showing the proinflammatory score of recruited macrophages. (*F–G*) Gene enrichment analysis (Gene Ontology [GO]) showed the top 20 pathways (*F*), and 2 of those are described by the enrichment score curve (*G*). (*H*) Heatmap of the differential number of interactions (FAH: n = 3 vs HBV: n = 3) between macrophages and T cells. (*I*) Cell–cell interaction probabilities from macrophage subsets to T cell subsets (the thickness of the line represents the strength of the interaction probability). $^{**}P < .01$; $^{****}P < .0001$. KC, Kupffer cell; Treg, regulatory T cell; Tfh, T follicular helper.

supported the contribution of CD8+ T cell exhaustion to viral persistence. Macrophages are known to have a dual facet in chronic HBV infection, such as playing antiviral and immunotolerant roles.[9] Macrophages from HBV-infected patients showed high levels of anti-inflammatory markers, and HBV exposure impaired the secretion of proinflammatory cytokines in macrophages.[9] Our CHB mice also showed suppression of pathways related to response to IFN-beta, regulation of defense response, immune response, and cytokine production in macrophages. The recent single-cell analysis revealed the heterogeneity of intrahepatic macrophages, and our CHB mice also had 2 subclusters in the macrophage population in the liver. In general, resident KCs are reported to be numerically decreased in the chronic inflammatory state.[27] In agreement with this, the numbers of resident KCs were reduced and those of recruited

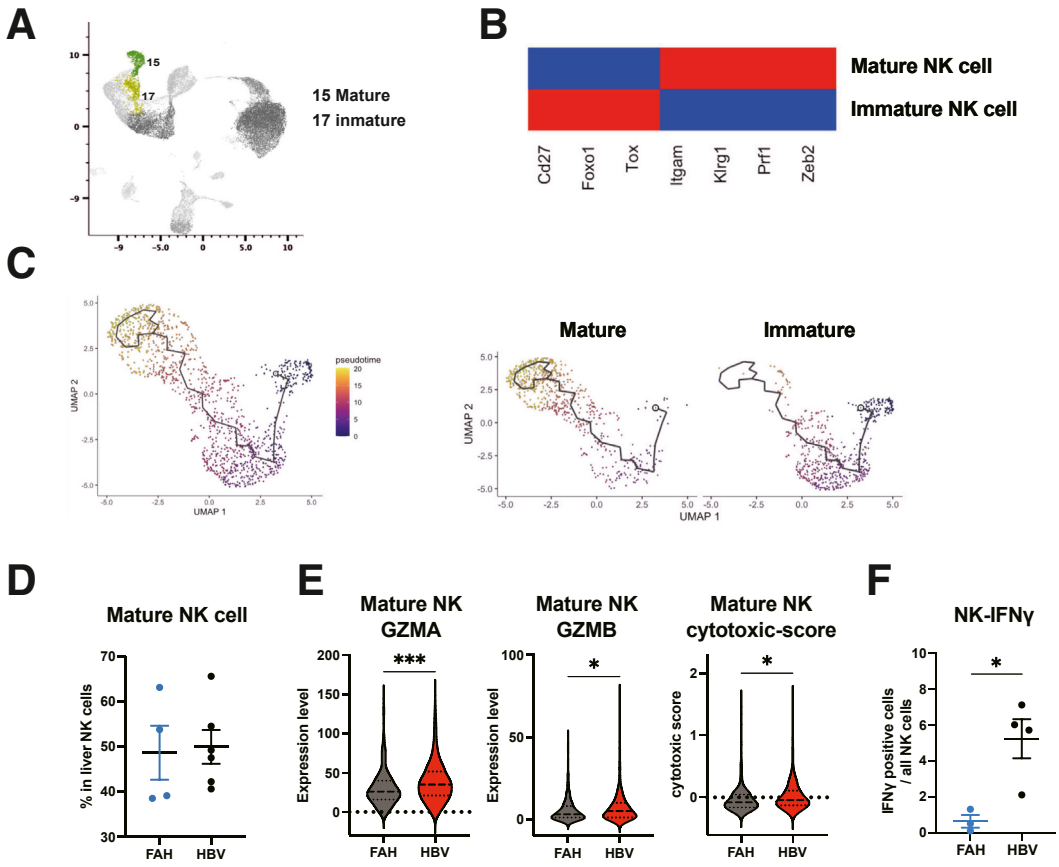

Figure 4. Activation of mature NK cells in the livers of CHB mice. (*A–E*) Hepatic immune cells from CHB mice and control mice at 8 weeks post-HTVi were analyzed by scRNA-seq sequencing (n = 6 for CHB mice and n = 4 for control mice). (*A–B*) Two NK cell subsets in UMAP (*A*) were defined by the indicated marker gene expression shown in the heatmap (*B*). (*C*) Pseudotime analysis of NK cell clusters. (*D*) Population of each cluster. (*E*) Violin plots showing the differentially expressed genes as indicated and the cytotoxic score of the mature NK cell cluster. (*F*) Frequency of IFNγ+ NK cells in the liver as determined by flow cytometry. *$P < .05$; ***$P < .001$.

macrophages were relatively increased in our CHB mice. Interestingly, our CHB mice showed a strong intrahepatic interaction between recruited macrophages and Tex cells. This finding suggests the involvement of recruited macrophages in CD8+ T cell exhaustion, which needs further investigation.

Currently, to maintain HBV persistence in the immunologically competent circumstance in mice, AAV-mediated HBV delivery was widely used. This AAV-HBV mouse model expressed most components of HBV and maintained HBV persistence more than 6 months.[28] In this model, HBV-specific CD8+ T cells were shown to be important for HBV elimination but exhausted.[29] Regarding macrophage population, F4/80$^+$ cells supported HBV persistence by inducing exhaustion of HBV-specific CD8+ T cells via TLR-2/IL-10 signaling.[30] In this model, it was also shown that NK cells were activated and NK cell-derived IFN-γ exerts anti-HBV function.[29] Our model also showed the exhaustion of HBV-specific CD8+ T cells, the impairment of the proinflammatory function of recruited macrophages, and their potential interaction, and NK cell activation, suggesting the similarity of intrahepatic immune status between the 2 CHB models.

Our CHB mice were able to profile the viral and intrahepatic immune kinetics upon treatment with immunomodulators. TLR7, a receptor for viral-derived RNA, is mainly expressed on pDCs, and this signaling activates innate and adaptive immunity.[31] TLR7 agonists are expected to be novel therapeutics for HBV treatment and have been utilized in a clinical trial on patients with CHB under NA treatment. However, viral control in serum evaluations is still unachieved.[32,33] SA-5 is a hepatotropic TLR-7 agonist that can be administered orally and delivered through the enterohepatic circulation into the liver, which is expected to prevent systemic adverse reactions. SA-5 is hepatotropic because this compound is a substrate of OATP1B1 and OATP1B3, both of which are transporters that are expressed on the sinusoidal membrane of hepatocytes. In the current study, SA-5 exerted an antiviral effect in CHB mice. Importantly, SA-5 induced not only innate immune responses, such as activation of macrophages and NK cells, but also adaptive immune responses through activation of exhausted CD8+ T cells. These findings may facilitate further clinical development of TLR-7 agonists targeting CHB and support the utility of our CHB mice as a platform of preclinical trials for patients with CHB.

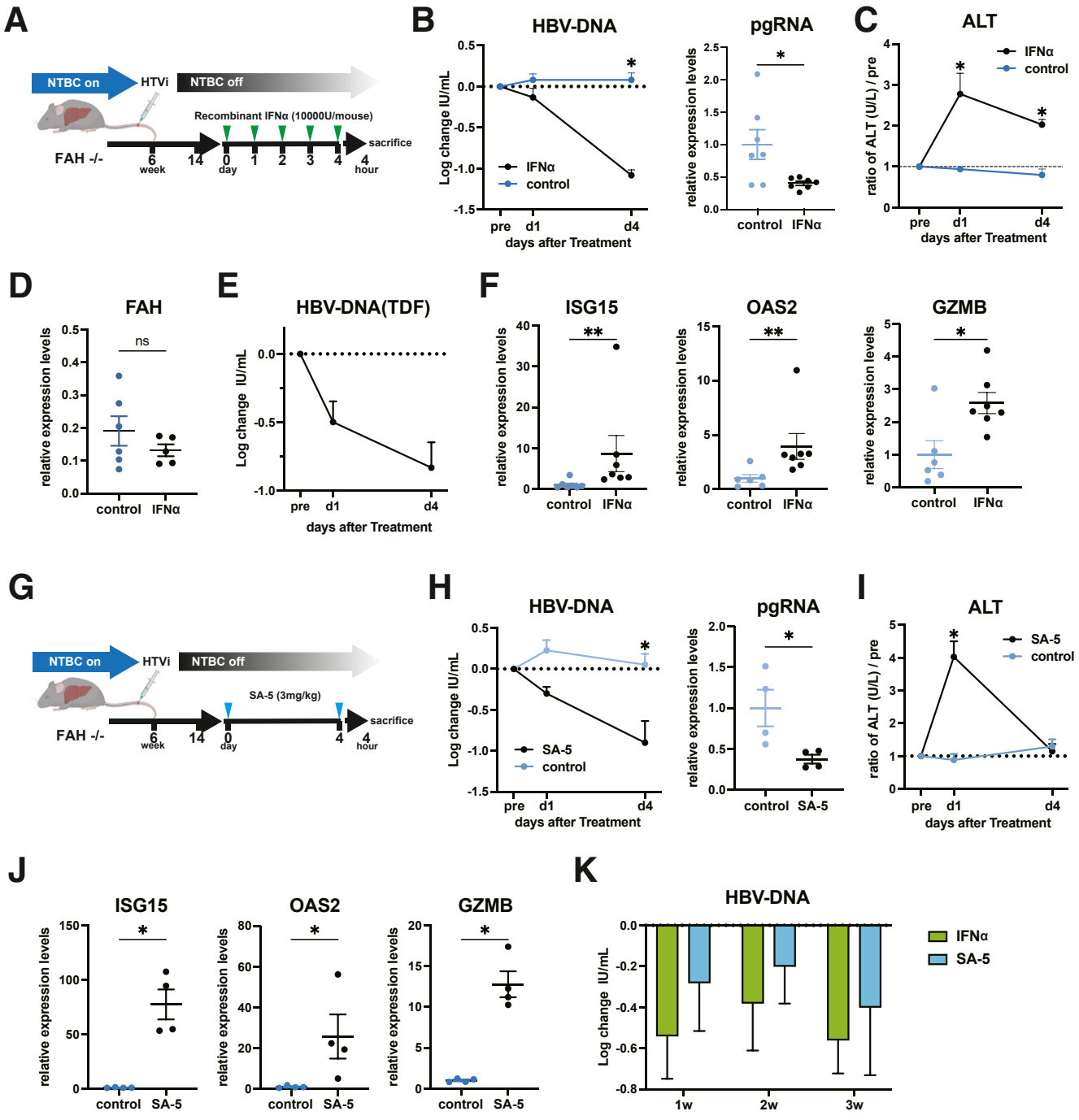

Figure 5. Immunomodulatory agents induce the intrahepatic immune response and viral suppression in CHB mice. (*A*) Experimental scheme. Recombinant IFNα (10,000 U/mouse, subcutaneous) or vehicle was administered daily to the CHB mice and the control mice at 8 weeks after HTVi (n = 7 mice per group). (*B*) Alterations in serum HBV-DNA levels compared with those at pretreatment and the intrahepatic pgRNA expression levels at the end of treatment. (*C*) Alteration in serum ALT levels compared with those at pretreatment. (*D*) FAH expression levels in the liver at the end of treatment. (*E*) Tenofovir disoproxil fumarate (TDF) (90 mg/kg orally every other day) was administered to the CHB mice at 8 weeks after HTVi (n = 3 mice per group). Alterations in serum HBV-DNA levels compared with those at pretreatment. (*F*) Intrahepatic mRNA expression levels of *Isg15*, *Oas2,* and *Gzmb* at the end of treatment. (*G*) Experimental scheme. The TLR7 agonist SA-5 (3 mg/kg orally) or vehicle was orally administered to CHB mice (n = 4 mice per group) at 8 weeks after HTVi. (*H*) Alteration of serum HBV-DNA levels compared with those at pretreatment and the intrahepatic pgRNA expression levels at the end of treatment. (*I*) Alteration in serum ALT levels compared with those at pretreatment. (*J*) Intrahepatic mRNA expression levels of *Isg15*, *Oas2* and *Gzmb* at the end of treatment. (*K*) Recombinant IFNα (10,000 U/mouse, subcutanously 3 times/week) or SA-5 (3 mg/kg orally weekly) or vehicle was administered to the CHB mice and the control mice for 3 weeks at 8 weeks after HTVi (n = 5 mice per group). Alterations in serum HBV-DNA levels compared with those at pretreatment. *$P < .05$; **$P < .01$.

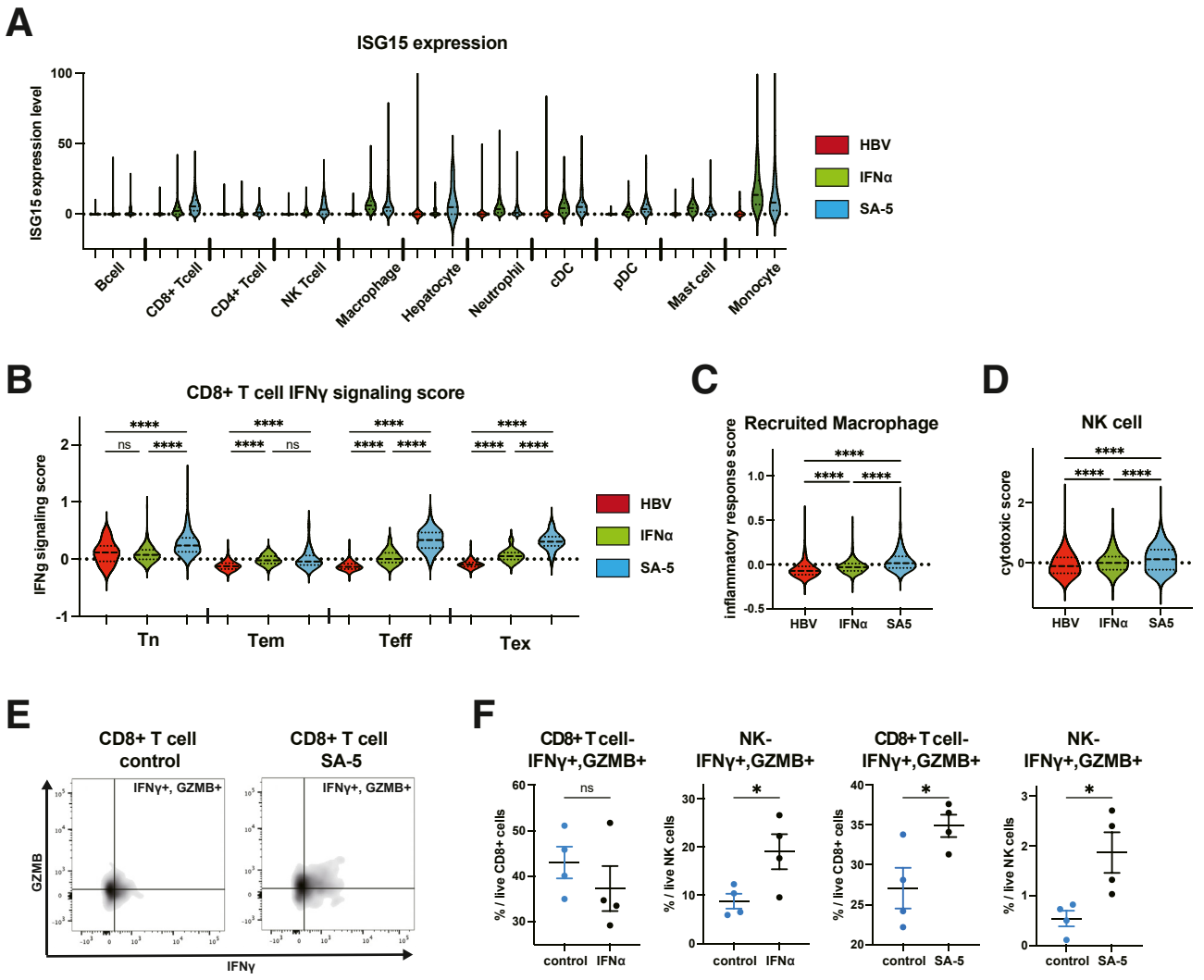

Figure 6. Immunomodulatory effects of IFNα and SA-5 in CHB mice. (*A–D*) Hepatic immune cells from CHB mice and control mice with IFNα or SA-5 treatment were analyzed by scRNA-seq sequencing (n = 3 mice per group). (*A*) Violin plots showing the ISG15 expression levels of each major cluster. (*B*) Violin plots showing the functional score (IFNγ signaling) of the indicated CD8+ T cell cluster. (*C*) Violin plots showing inflammatory response scores of recruited macrophages. (*D*) Violin plots showing cytotoxic scores of NK cell. (*E*) Representative dot plots of IFNγ+GZMB+ CD8+ T cells in the liver as determined by flow cytometry. (*F*) Frequencies of intrahepatic IFNγ+GZMB+ CD8+ T and IFNγ+GZMB+ NK cells as determined by flow cytometry. $^{*}P < .05$; $^{****}P < .0001$.

Our model has certain limitations. The clinical course of human HBV infection was not fully recapitulated in our mice model. ALT flares occur during major virus replication in our model, but it generally occurs at the end of the acute phase in humans. Although we did not see the apparent inflammatory response in the liver of FAH KO mice with exogenous hepatic FAH expression upon withdrawal of drinking NTBC, it is not able to fully eliminate the possibility of interference between immunity to HBV and exogenous FAH in our model.

In conclusion, with a combination of a FAH-KO mouse, HTVi, and SB transposon system, we have succeeded in establishing a novel CHB mouse model recapitulating the intrahepatic exhausted anti-viral immunity in patients with CHB, which can be reinvigorated by a hepatotropic TLR7 agonist.

Materials and Methods

DNA Constructs

Plasmids containing the 1.24-mer overall length of the genotype-A HBV genome (Ae_US; GenBank accession no. AB246337), 1.30-mer overall length of genotype-C (C_JPN22; GenBank accession no. AB246344) HBV genome (from Prof. Y. Tanaka), FAH cDNA (from Dr. Keng Vincent at The Hong Kong Polytechnic University: described in A Wilber et al[34]), and pT2/BH (a gift from Perry Hackett: Addgene plasmid # 26556; http://n2t.net/addgene:26556 ; RRID:Addgene_26556) were used. The core 93 epitope of the genotype-C HBV genome has a single nucleotide mutation to express the known CD8+ T-cell epitope (MGLKFRQL) described in Kawashima et al.[35] The HBV genome, CMV promoter-driven FAH cDNA, or both together

were cloned into a single SB transposon vector (pT2/BH) (called SB-HBV, SB-FAH, SB-HBV-FAH, respectively).

Mice

The animal procedures and maintenance were approved by the Animal Care and Use Committee of Osaka University Medical School (Osaka, Japan). FAH-KO mice were provided by RIKEN (RBRC05362) and backcrossed to C57BL/6 mice. FAH-KO mice were maintained with NTBC (2-[2-nitro-4-[1] benzoyl]cyclohexane-1,3-dione) at 16 mg per 1 liter drinking water to prevent lethal hepatic damage.

Hydrodynamic Injection

Vectors were manufactured using the QIAGEN EndoFree Maxi Kit (#12362; QIAGEN). Via HTVi, each SB transposon vector (40 μg/mouse) along with SB transposase (#34879; pCMV(CAT)T7-SB100 obtained from Addgene, 8 μg/mouse) in saline with a volume of 10% of the mouse body weight was introduced into the mice at the age of 6 to 7 weeks. After HTVi, NTBC was withdrawn, and normal water was given to the mice.

Evaluation of HBV Expression and Hepatic Damage

To evaluate serum HBV expression, blood was collected from the jugular vein of the mouse weekly. Serum levels of HBV DNA, HBeAg, and HBsAg were measured by a standard method at SRL, Inc. To detect pregenomic RNA (pgRNA), total RNA isolated from liver tissues at 30 weeks after HTVi using an RNeasy Mini Kit (#74104; Qiagen) with DNase (#79254; Qiagen) was reverse-transcribed and subjected to real-time reverse transcription PCR (RT−PCR) with the primers manufactured by Applied Biosystems (Probe: 5′-FAM CATGGACATTGACCC-3′, Forward primer: 5′- TGTCCTACT-GTTCAAGCCTCCAA-3′, Reverse primer: 5′-GAGAGTAACTCCA-CAGAAGCTC CAA-3′). The mRNA expression levels were quantified using TaqMan Gene Expression Assays (Thermo Fisher Scientific) (Table 1). Serum ALT was measured by a standard method at Oriental Yeast Co. Serum caspase-3/7 activity was measured by luminescent substrate assay (#G8090; Promega) at 30 weeks after HTVi.

Histologic Analyses

Formalin-fixed and paraffin-embedded liver sections at 20 weeks after HTVi were stained with hematoxylin and eosin (H&E). We performed immunostaining by applying anti-HBs antibody (bs-1557G: Bioss Antibodies) or FAH (ab83770: Abcam) for primary staining after heat-induced epitope retrieval, followed by secondary staining using ABC kit (PK-6105/PK-4001: VEC) and then carried out DAB color development. Inflammatory cells were automatically detected and quantified on H&E staining using the image analysis system HALO (IndicaLabs: AreaQuantification v2.1.11).

Table 1. List of Primer Sets for RT-qPCR

Gene name	Manufacturer
Mouseβ-actin	Thermo Fisher Scientific (Mm02619580_g1)
Mouse ISG15	Thermo Fisher Scientific (Mm01705338_s1)
Mouse OAS2	Thermo Fisher Scientific (Mm00460961_m1)
Mouse GZMB	Thermo Fisher Scientific (Mm00442837_m1)
Mouse FAH	Thermo Fisher Scientific (Mm00487336_m1)

RT-PCR, Reverse transcription polymerase chain reaction.

Single-cell Preparation and Flow Cytometric Analysis

Intrahepatic mononuclear cells (MNCs) were isolated from perfused livers using 10 mL phosphate buffered saline (PBS) followed by filtering through a 70-μM cell strainer and gradient centrifugation on Percoll (40% and 70% Percoll, #17089101; Cytiva). MNCs from spleens were also filtered through a 70-μM cell strainer (#352350; Corning) and resuspended in red blood cell (RBC) lysis buffer (0.0776 M of ammonium chloride and 0.0851 M of Tris adjusted to pH 7.65, mixed in a ratio of 9:1). DimerX (Table 2) for the detection of HBV-specific CD8+ T cells was prepared by pre-mixing with Core93 peptide (MGLKFRQL), purchased from Scrum, in equal amounts and incubating at 4 °C overnight or longer. In the CD8+ T cell panel (Table 2), MNCs were incubated at 4 °C for 20 minutes with the prepared DimerX, monoclonal antibody (mAb) of CD8a, CD279, and CD366. Subsequently, incubation was carried out at 4 °C for 20 minutes with anti-mouse IgG (secondary staining for DimerX), followed by staining with 7-aminoactinomycin D (7AAD) for 15 minutes, and evaluation using flow cytometry with a FACSCanto II (Becton Dickinson). The tetramer panel (Table 2) was initially stained at room temperature for 60 minutes with HBc-Tetramer (MGLKFRQL) and HBs-Tetramer (VWLSVIWM). Subsequently, staining with mAb of CD3e, CD4, and CD8 was performed at room temperature for 15 minutes. Prior to flow cytometry analysis using fluorescence-activated cell sorting (FACS), dead cell staining was conducted with 7-AAD.

Intracellular Cytokine Staining

The cytokine expression of CD8+ T cells and NK cells was evaluated using intracellular cytokine staining. Cells were stimulated with ionomycin (5 μg/mL, #I0634-1MG; Sigma Aldrich) and phorbol myristate acetate (PMA) (30 ng/mL, #P8139-1MG; Sigma Aldrich) in the presence of GolgiStop Protein Transport Inhibitor containing monensin (0.66 μL/mL, # 554715; Becton Dickinson) for 4 hours and incubated with Fixable Viability Stain 780 for 15 minutes. After staining with mAb of CD8a and prepared DimerX (secondary staining with anti-mouse IgG as describe above) for cytokine staining Panel 1 (Table 2), or with mAb of CD3e, CD8a, and CD49b for cytokine staining Panel 2 (Table 2), for 20 minutes, the cells were fixed and permeabilized with fixation/permeabilization solution (BD #554715) for 20 minutes at room temperature and stained with TNFα and IFNγ for cytokine staining Panel 1, or with

Table 2. List of Antibodies for FACS Analysis

Antigen	Fluorochrome	Clone	Manufacturer
CD8+ T cell panel			
7-AAD	PerCP/Cy5.5		BD Bioscience (559925)
CD8a	APC/H7	53-6.7	BD Bioscience (560247)
DimerX(H-2K[b]:Ig)	-		BD Bioscience (550750)
Anti-mouse IgG1	FITC	A85-1	BD Bioscience (553443)
CD279	BV421	J43	BD Bioscience (565942)
CD366	PE-Cy7	RMT3-23	Biolegend (119715)
Tetramer panel			
7-AAD	PerCP/Cy5.5		BD Bioscience (559925)
H2kb-HBc-Tetramer	PE		MBL TB-M537-1
H2kb-HBs-Tetramer	Bv421		MBL TB-5110-4
CD3e	BV510	145-2C11	BD Bioscience (563024)
CD4	FITC	GK1.5	BD Bioscience (553729)
CD8	AF647	KT15	MBL K0227-A67
Cytokine staining panel 1			
Fixable Viability Stain 780	APC/Cy7		BD Bioscience (565388)
CD8a	APC	53-6.7	Biolegend (100711)
DimerX(H-2K[b]:Ig)	-		BD Bioscience (550750)
Anti-mouse IgG1	FITC	A85-1	BD Bioscience (553443)
TNFα	PerCP/Cy5.5	MP6-XT22	BD Bioscience (560659)
IFNγ	AF488	XMG1.2	BD Bioscience (557724)
Cytokine staining panel 2			
Fixable Viability Stain 780	APC/Cy7		BD Bioscience (565388)
CD3e	BV510	145-2C11	BD Bioscience (563024)
CD8a	APC	53-6.7	Biolegend (100711)
CD49b	PE	DX5	BD Bioscience (553858)
IFNγ	AF488	XMG1.2	BD Bioscience (557724)
GZMB	BV421	QA18A28	Biolegend (396414)

FACS, Fluorescence-activated cell sorting.

IFNγ and GZMB for cytokine staining Panel 2. The stained cells were acquired on a FACS Canto II as described above. The data were analyzed using FlowJo (Becton Dickinson).

Single-cell RNA Sequencing

MNCs were isolated from the liver as in the flow cytometric analysis. For scRNA-seq, we utilized the BD Rhapsody system (Becton Dickinson). MNCs were labelled with sample tags (Ms Single Cell Sample Multiplexing Kit), counted, and multiplexed. Cell capture and library preparation were performed using the BD Rhapsody Whole Transcriptome Analysis (WTA) Reagent Kit (Becton Dickinson) following the manufacturer's protocol, and libraries were sequenced on MGI Tech DNBSEQ-G400RS. The FASTQ files from the sequences were processed using the BD Rhapsody WTA Pipeline v1.10.1 (Becton Dickinson) in the Seven Bridges Platform. The data on the number of molecules from the Seven Bridges Platform were further analyzed with SeqGeq v1.8.0. Through quality control, cells with significantly smaller library sizes and fewer expressed genes were excluded as dead cells. Then, dimensional reduction (uniform manifold approximation and projection [UMAP]) and clustering were performed using the Seurat plug-in implementing Seurat v4.3.0,[36] which includes scTransform for normalization and variance stabilization of molecular count data. To determine the optimal number of clusters, the clustering process was repeated with varying resolution parameters from 0.2 to 2 in increments of 0.2, and the adopted clustering was determined based on the classification of CD8+ T-cell subtypes. Cell annotations were determined by manually checking the known marker gene expression in each cell cluster. For deeper analysis, gene expression data for each cell cluster were exported from SeqGeq and processed with the R package clusterProfiler v4.4.4[37] for GSEA, Monocle 3 v1.2.7, and CellChat v1.4.0.[38] Functional scores were calculated as the mean expression of relevant genes (normalized by z score). The enrichment score was calculated by GSEA.[39] Gene sets for exhaustion, proinflammatory, and NK cytotoxic scores were extracted from Zhang et al.[26] The IFNγ response score and macrophage inflammatory response was defined as in mouse-orthologue hallmark (MSigDB, Broad Institute).

Compounds

NTBC and recombinant IFNα were purchased from Toronto Research Chemicals, Inc (#N490135-1g) and PBL Assay Science (#12100-1), respectively. SA-5 (TLR-7 agonist) was compounded by Sumitomo Pharma Co., Ltd. Recombinant IFNα solution was diluted in PBS before injection, and SA-5 was administered with 0.5 wt%/vol% Methyl Cellulose 400 Solution (#133-17815; Fujifilm Wako Pure Chemical Corp). Tenozevir (Tenofovir Disoproxil Fumarate) was obtained from GlaxoSmithKline.

Integrated Copy Number Measurement

DNA was extracted from mouse liver using the QIAamp DNA Mini kit (QIAGEN #51306). Based on the report by Kolacsek et al,[40] PCR was performed using a probe specific for the SB transposon-delivered transgene sequence IR/DR-L (Probe: 5′-FAM CTGACTTGCCAAAACT, PrimerF: CTCG TTTTTCAACTACTCCACAAATTTCT, PrimerR: GTGTCATGCA-CAAAGTAGATGTCCTA). CT values were determined by qPCR. Simultaneously, the copy number reference was measured using the TaqMan Copy Number Reference Assay for mouse Tfrc (Thermo, 4458366). The expression ratio of IR/DR-L to Tfrc was adjusted based on the FAH-positive population identified by histological staining.

pgRNA Copy Number Measurement

cDNA synthesized from extracted RNA was subjected to digital PCR assay using the same probe as in qPCR on the ThermoFisher QuantStudio Absolute Q. Negative controls were concurrently measured to establish thresholds.

Statistical Analysis

All data are expressed as the mean ± standard error of the mean (SEM). To assess the significant differences between 2 groups, 2-tailed Student's *t*-test was performed. A P value $< .05$ was considered to indicate statistical significance. One-way analysis of variance (ANOVA) with Tukey's multiple comparisons test was used to compare more than 2 groups. Statistical analysis was performed with GraphPad Prism 9 v9.4.1 (GraphPad Software, LLC).

References

1. World Health Organization. Fact sheet, Hepatitis B. 2022; June, Available at: https://www.who.int/news-room/fact-sheets/detail/hepatitis-b. Accessed February 17, 2023.
2. McMahon BJ. The natural history of chronic hepatitis B virus infection. Hepatology 2009;49:S45–S55.
3. Terrault NA, Bzowej NH, Chang KM, et al, American Association for the Study of Liver Diseases. AASLD guidelines for treatment of chronic hepatitis B. Hepatology 2016;63:261–283.
4. European Association for the Study of the Liver. EASL 2017 Clinical Practice Guidelines on the management of hepatitis B virus infection. J Hepatol 2017;67:370–398.
5. Fanning GC, Zoulim F, Hou JL, Bertoletti A. Therapeutic strategies for hepatitis B virus infection: towards a cure. Nat Rev Drug Discov 2019;18:827–844.
6. Nguyen MH, Wong G, Gane E, et al. Hepatitis B virus: advances in prevention, diagnosis, and therapy. Clin Microbiol Rev 2020;33:e00046-19.
7. Gehring AJ, Protzer U. Targeting innate and adaptive immune responses to cure chronic HBV infection. Gastroenterology 2019;156:325–337.
8. Schuch A, Alizei ES, Heim K, et al. Phenotypic and functional differences of HBV core-specific versus HBV polymerase-specific CD8+T cells in chronically HBV-infected patients with low viral load. Gut 2019; 68:905–915.
9. Li YJ, Li SL, Duan XQ, et al. Macrophage phenotypes and hepatitis B virus infection. J Clin Transl Hepatol 2020;8:424–431.
10. Li YM, Zhu YW, Feng S, et al. Macrophages activated by hepatitis B virus have distinct metabolic profiles and suppress the virus via IL-1 beta to downregulate PPAR alpha and FOXO3. Cell Reports 2022;38:111068.
11. Liu YZ, Maya S, Ploss A. Animal models of hepatitis B virus infection-success, challenges, and future directions. Viruses-Basel 2021;13:777.
12. Allweiss L, Dandri M. Experimental in vitro and in vivo models for the study of human hepatitis B virus infection. J Hepatol 2016;64:S17–S31.
13. Burwitz BJ, Zhou ZM, Li WH. Animal models for the study of human hepatitis B and D virus infection: new insights and progress. Antiviral Research 2020;182:104898.
14. Yang D, Liu LC, Zhu DM, et al. A mouse model for HBV immunotolerance and immunotherapy. Cell Mol Immunol 2014;11:71–78.
15. Kawashima K, Isogawa M, Onishi M, et al. Restoration of type I interferon signaling in intrahepatically primed CD8(+) T cells promotes functions differentiation. JCI Insight 2021;6:e145761.
16. Sun SW, Li J. Humanized chimeric mouse models of hepatitis B virus infection. Int J Infect Dis 2017; 59:131–136.
17. Lai F, Wee CYY, Chen QF. Establishment of humanized mice for the study of HBV. Front Immunol 2021;12: 638447.
18. Yuan LZ, Jiang J, Liu X, et al. HBV infection-induced liver cirrhosis development in dual-humanised mice with human bone mesenchymal stem cell transplantation. Gut 2019;68:2044–2056.
19. Trapnell C, Cacchiarelli D, Grimsby J, et al. The dynamics and regulators of cell fate decisions are revealed by pseudotemporal ordering of single cells. Nat Biotechnol 2014;32:381–386.
20. Ota Y, Nagai Y, Hirose Y, et al. DSP-0509, a systemically available TLR7 agonist, exhibits combination effect with immune checkpoint blockade by activating anti-tumor immune effects. Front Immunol 2023;14:1055671.
21. Park JH, Iwamoto M, Yun JH, et al. Structural insights into the HBV receptor and bile acid transporter NTCP. Nature 2022;606:1027–1031.
22. Grompe M. Fah knockout animals as models for therapeutic liver repopulation. Adv Exp Med Biol 2017; 959:215–230.
23. Ghany MG, Lok AS. Functional cure of hepatitis B requires silencing covalently closed circular and integrated hepatitis B virus DNA. J Clin Invest 2022;132:e163175.
24. Yang PL, Althage A, Chung J, et al. Immune effectors required for hepatitis B virus clearance. Proc Natl Acad Sci U S A 2010;107:798–802.
25. Ye B, Liu X, Li X, et al. T-cell exhaustion in chronic hepatitis B infection: current knowledge and clinical significance. Cell Death Dis 2015;6:e1694.
26. Zhang C, Li J, Cheng Y, et al. Single-cell RNA sequencing reveals intrahepatic and peripheral immune characteristics related to disease phases in HBV-infected patients. Gut 2023;72:153–167.

27. Zwicker C, Bujko A, Scott CL. Hepatic macrophage responses in inflammation, a function of plasticity, heterogeneity or both? Front Immunol 2021;12:690813.
28. Ye L, Yu H, Li C, et al. Adeno-associated virus vector mediated delivery of the HBV genome induces chronic hepatitis B virus infection and liver fibrosis in mice. PLoS One 2015;10:e0130052.
29. Zheng M, Sun R, Wei H, Tian Z. NK cells help induce anti-hepatitis B virus CD8+ T cell immunity in mice. J Immunol 2016;196:4122–4131.
30. Li M, Sun R, Xu L, et al. Kupffer cells support hepatitis B virus-mediated CD8+ T cell exhaustion via hepatitis B core antigen-TLR2 interactions in mice. J Immunol 2015; 195:3100–3109.
31. Takagi H, Arimura K, Uto T, et al. Plasmacytoid dendritic cells orchestrate TLR7-mediated innate and adaptive immunity for the initiation of autoimmune inflammation. Sci Rep 2016;6:24477.
32. Yuen MF, Balabanska R, Cottreel E, et al. TLR7 agonist RO7020531 versus placebo in healthy volunteers and patients with chronic hepatitis B virus infection: a randomised, observer-blind, placebo-controlled, phase 1 trial. Lancet Infect Dis 2023;23:496–507.
33. Boni C, Vecchi A, Rossi M, et al. TLR7 agonist increases responses of hepatitis B virus-specific T cells and natural killer cells in patients with chronic hepatitis B treated with nucleos(T)Ide analogues. Gastroenterology 2018; 154:1764–1777.e7.
34. Wilber A, Wangensteen KJ, Chen Y, et al. Messenger RNA as a source of transposase for sleeping beauty transposon–mediated correction of hereditary tyrosinemia type I. Mol Ther 2007;15:1280–1287.
35. Kawashima K, Isogawa M, Hamada-Tsutsumi S, et al. Type I interferon signaling prevents hepatitis B virus-specific T cell responses by reducing antigen expression. J Virol 2018;92:e01099-18.
36. Butler A, Hoffman P, Smibert P, et al. Integrating single-cell transcriptomic data across different conditions, technologies, and species. Nat Biotechnol 2018; 36:411–420.
37. Wu TZ, Hu EQ, Xu SB, et al. clusterProfiler 4.0: a universal enrichment tool for interpreting omics data. Innovation (Camb) 2021;2:100141.
38. Jin SQ, Guerrero-Juarez CF, Zhang LH, et al. Inference and analysis of cell-cell communication using CellChat. Nat Commun 2021;12:1088.
39. Subramanian A, Tamayo P, Mootha VK, et al. Gene set enrichment analysis: a knowledge-based approach for interpreting genome-wide expression profiles. Proc Natl Acad Sci U S A 2005;102:15545–15550.
40. Kolacsek O, Krizsik V, Schamberger A, et al. Reliable transgene-independent method for determining Sleeping Beauty transposon copy numbers. Mob DNA 2011;2:5.

Received November 21, 2023. Accepted September 23, 2024.

Correspondence
Address correspondence to: Tetsuo Takehara, MD, PhD, 2-2 Yamadaoka Suita, Osaka 565-0871, Japan. e-mail: takehara@gh.med.osaka-u.ac.jp.

Acknowledgements
The genotype-C HBV genome was kindly provided by Prof Yasuhito Tanaka (Nagoya City University, Kumamoto University). The authors thank Dr Keisuke Fukutomi, Ms Miyuki Imai, Ms Yoko Sato, Dr Yu Sato, and Dr Akiyoshi Shimoda for their experimental help.

CRediT Authorship Contributions
Satoshi Shigeno (Data curation: Lead; Formal analysis: Lead; Methodology: Lead; Validation: Lead; Visualization: Lead; Writing – original draft: Lead)
Takahiro Kodama (Conceptualization: Lead; Formal analysis: Equal; Funding acquisition: Lead; Validation: Equal; Visualization: Equal; Writing – original draft: Equal)
Kazuhiro Murai (Formal analysis: Supporting; Methodology: Supporting)
Daisuke Motooka (Formal analysis: Supporting; Writing – original draft: Supporting)
Akihisa Fukushima (Formal analysis: Supporting; Methodology: Supporting)
Akira Nishio (Formal analysis: Supporting; Methodology: Supporting)
Hayato Hikita (Formal analysis: Supporting; Methodology: Supporting)
Tomohide Tatsumi (Formal analysis: Supporting; Methodology: Supporting)
Toru Okamoto (Formal analysis: Supporting; Methodology: Supporting)
Tatsuya Kanto (Formal analysis: Supporting; Methodology: Supporting)
Tetsuo Takehara, MD, PhD (Formal analysis: Supporting; Funding acquisition: Equal; Supervision: Lead; Writing – review & editing: Lead)

Conflicts of interest
These authors disclose the following: Tetsuo Takehara, Takahiro Kodama, and Satoshi Shigeno received grants from Shionogi & Co., Ltd. Akihisa Fukushima is a full-time employee of Sumitomo Pharma Co., Ltd. The remaining authors disclose no conflicts.

Funding
Generation of the mouse model was supported by the Japan Agency for Medical Research and Development (AMED) under grant numbers JP24fk0310512 (Hayato Hikita and Tetsuo Takehara) and JP21fk0310106 (Takahiro Kodama), JP24fk0210131 (Takahiro Kodama). Validation of the mouse model was supported by Shionogi & Co., Ltd. Single-cell sequence-based evaluation of the mouse model and the profiling of the immune responses to the immunomodulators were supported by the Japan Agency for Medical Research and Development (AMED) under grant numbers JP21fk0310106 (Takahiro Kodama, Tatsuya Kanto), JP22fk0310524 (Takahiro Kodama), JP22fk0210110 (Takahiro Kodama), and JP24ama221410 (Takahiro Kodama).

Data Availability
Raw data and processed data of single cell RNA sequence of immune cells in mice were deposited in Gene Expression Omnibus (GEO) database (GSE271816).